

### Search for the Decay $K^+ \rightarrow \pi^+ \nu \bar{\nu}$

M. S. Atiya, I.-H. Chiang, J. S. Frank, J. S. Haggerty, M. M. Ito, T. F. Kycia, K. K. Li, L. S. Littenberg, A. Stevens, and R. C. Strand

*Brookhaven National Laboratory, Upton, New York 11973*

W. C. Louis

*Medium Energy Physics Division, Los Alamos National Laboratory, Los Alamos, New Mexico 87545*

D. S. Akerib, D. R. Marlow, P. D. Meyers, M. A. Selen, F. C. Shoemaker, and A. J. S. Smith

*Joseph Henry Laboratories, Princeton University, Princeton, New Jersey 08544*

G. Azuelos, E. W. Blackmore, D. A. Bryman, L. Felawka, P. Kitching, Y. Kuno, J. A. Macdonald,

T. Numao, P. Padley, J.-M. Poutissou, R. Poutissou, and J. Roy

*TRIUMF, Vancouver, British Columbia, Canada V6T 2A3*

(Received 2 October 1989)

An upper limit on the branching ratio for the decay  $K^+ \rightarrow \pi^+ \nu \bar{\nu}$  is set at  $3.4 \times 10^{-8}$  (90% C.L.). In addition, a 90%-C.L. upper limit of  $6.4 \times 10^{-9}$  is set on the branching ratio for decays of the form  $K^+ \rightarrow \pi^+ X^0$ , where  $X^0$  is any massless, weakly interacting neutral particle. Limits are also set for the case where  $M_{X^0} > 0$ .

PACS numbers: 13.20.Eb, 12.15.Ji, 14.80.Gt, 14.80.Ly

In this Letter we report results from Brookhaven Experiment 787, which is sensitive to all processes of the form  $K^+ \rightarrow \pi^+ X^0$ , where  $X^0$  is any light, weakly interacting neutral or system of neutrals. The reaction  $K^+ \rightarrow \pi^+ \nu \bar{\nu}$  is of particular interest, since it is a prime example of a flavor-changing neutral-current (FCNC) process. In the standard model (SM), FCNC processes are forbidden to lowest order by the Glashow-Iliopoulos-Maiani (GIM) mechanism,<sup>1</sup> but can proceed via higher-order weak diagrams, where mass differences between the internal quarks spoil the GIM cancellation. The six-quark SM prediction<sup>2,3</sup> for the branching ratio lies in the range  $B(K^+ \rightarrow \pi^+ \nu \bar{\nu}) \simeq (1-8) \times 10^{-10}$ , depending upon the top-quark mass and the Kobayashi-Maskawa matrix elements.<sup>4</sup> The previous experimental upper limit<sup>5</sup> is  $B(K^+ \rightarrow \pi^+ \nu \bar{\nu}) < 1.4 \times 10^{-7}$  (90% C.L.).

Alternatively,  $X^0$  might represent a pair of light supersymmetric particles<sup>6</sup> or a pair of majorons.<sup>7</sup> Single-particle possibilities for  $X^0$  include light Higgs particles and Goldstone bosons, such as the familon<sup>8</sup> particle postulated as a by-product of the spontaneous breakdown of family symmetry.

The one-charged-track signature of  $K^+ \rightarrow \pi^+ \nu \bar{\nu}$  is dominated by backgrounds from the common two-body decays  $K^+ \rightarrow \mu^+ \nu$  and  $K^+ \rightarrow \pi^+ \pi^0$ , which, for kaons at rest, have recoil momenta of 236 and 205 MeV/c, respectively. Below 205 MeV/c, the  $K^+ \rightarrow \pi^+ \nu \bar{\nu}$  spectrum is contaminated by  $K^+ \rightarrow \pi^+ \pi^0$  decays where the decay pion is shifted down in energy by nuclear interactions in the material of the detector, leading us to restrict our search to the region between 205 MeV/c and the 227-MeV/c end point of the  $K^+ \rightarrow \pi^+ \nu \bar{\nu}$  spectrum. In-

dependent measurements of the momentum, energy, and range of the charged track gave a large degree of redundancy in determining the kinematics of each decay. Further background suppression was gained by the ability to reject events with photons and to identify charged pions by detecting their characteristic  $\pi^+ \rightarrow \mu^+ \rightarrow e^+$  decay chain. This strategy also suppressed backgrounds from other decays, notably  $K^+ \rightarrow \mu^+ \nu \gamma$ ,  $K^+ \rightarrow \pi^0 \mu^+ \nu$ , and  $K^+ \rightarrow 3\pi$ .

The cylindrically symmetric detector,<sup>9</sup> shown in Fig. 1, rests in a 3-m-inner-diam conventional solenoidal magnet that produces a field of 1 T. Positive kaons from the Low Energy Separated Beam (LESB I) at the Alternating Gradient Synchrotron (AGS) entered the apparatus at a momentum of 775 MeV/c through a set of beam-defining scintillators and a Lucite-radiator Čerenkov counter, designed to independently tag  $K^+$ 's and veto  $\pi^+$ 's. The beam  $\pi:K$  ratio was approximately 2.5:1. The kaons were slowed in a BeO degrader and a scintillator hodoscope (B4) before being stopped in a hexagonal target formed from scintillating fibers.<sup>10</sup> In a typical 1.8-s AGS spill,  $8 \times 10^5$  kaons entered the degrader, of which  $1.5 \times 10^5$  were stopped in the target.

The 3-m-long, 2-mm-diam target fibers were grouped into 379 triangular clusters of six, each viewed by a 1-cm-diam photomultiplier tube. A combination of pulse-height (energy) and leading-edge timing information from the target clusters was used to track both the incident  $K^+$  and the decay  $\pi^+$ . An array of six 20-cm-long, 6-mm-thick plastic scintillators ( $I$  counters) surrounding the target defined the fiducial stopping volume.

Charged-particle momenta were measured in a cylindrical drift chamber<sup>11</sup> having 1536 sense wires arranged

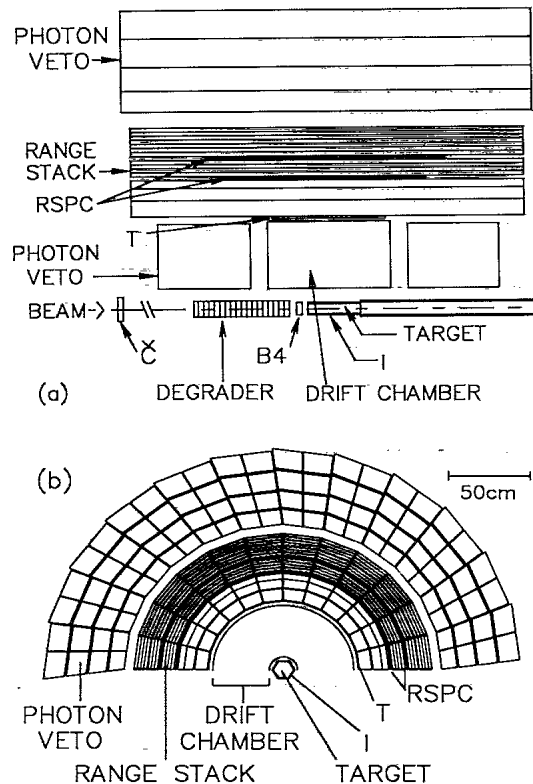


FIG. 1. Schematic (a) side and (b) end views showing the upper half of the E787 detector.

in five superlayers of six-wire cells. The wires of the second and fourth superlayers were inclined at approximately  $\pm 4^\circ$  to provide stereo views for  $z$  measurement.

The decay pions were stopped in a segmented plastic-scintillator range stack that surrounded the drift chamber. The range stack measured the energy and range of the stopping pions. The counters of the innermost layer ( $T$  counters) defined the approximately  $2\pi$  charged-particle detection solid angle. The counters in the region where the pions of interest stopped (layers 5–12) were 1.95 cm thick and were viewed from each end by 5-cm-diam phototubes. Two layers of multiwire proportional chambers (RSPC's) were embedded in the range stack to provide additional measurements of the trajectories of the pions as they came to rest.

Range-stack counters in the pion stopping region were instrumented with transient digitizers<sup>12</sup> (TD's), which performed an eight-bit digitization of the phototube outputs every 2 ns. All nonzero TD outputs occurring within  $\pm 5 \mu\text{s}$  of the kaon decay time were recorded, providing pulse-shape information for the  $\pi^+ \rightarrow \mu^+ \rightarrow e^+$  analysis along with a complete history of range-stack activity.

Photons were detected in a segmented 14-radiation-length-thick lead-scintillator (1 mm lead–5 mm scintillator) array surrounding the range stack and in a pair of segmented lead-scintillator end caps. Together, these

systems provided a nearly  $4\pi$  photon detection solid angle.

The trigger logic was arranged in three levels of increasing complexity and decision time. Level 0 required an  $I$ -counter signal, delayed by at least 2 ns with respect to the  $K^+$  stopping time, as well as a coincidence between the inner three layers of the range stack.  $K^+ \rightarrow \mu^+ \nu$  decays were rejected by vetoing events that penetrated to the outer three layers of the range stack.  $K^+ \rightarrow \pi^+ \pi^0$  and  $K^+ \rightarrow \pi^0 \mu^+ \nu$  decays were rejected by vetoing all events with more than  $\approx 5$  MeV of visible energy in the photon detectors. Additional  $K^+ \rightarrow \mu^+ \nu$  rejection was obtained in levels 1 and 2. Level 1 refined the coarse range cut of level 0 by taking into account the track angle, determined from the RSPC  $z$  measurement, and the target path length, determined by counting the number of struck target clusters. Level 2 used a microprocessor to sum the energies deposited by the decay track in the target and the range stack. Events with charged-track energies greater than 142 MeV were rejected. Level 2 also examined the TD data from the  $\pi^+$  stopping counter for evidence of a second pulse arising from  $\pi^+ \rightarrow \mu^+ \nu$  decay. Events lacking a separated second pulse and having a pulse area-to-height ratio consistent with a single stopping particle were rejected. In a typical spill of  $1.5 \times 10^5$  stopping  $K^+$ 's, the number of surviving  $K^+ \rightarrow \pi^+ \nu \bar{\nu}$  triggers was 6800, 450, and 15, after levels 0, 1, and 2, respectively. The live time of the data acquisition system was typically 70%. In total,  $2.6 \times 10^6$   $K^+ \rightarrow \pi^+ \nu \bar{\nu}$  level-2 triggers were recorded.

The off-line analysis program searched for events with a single matching  $\pi^+$  track in the target, drift chamber, and range stack. After correcting for energy loss and path length in the target, the (rms) resolutions of the momentum, kinetic-energy, and range measurements at the  $K^+ \rightarrow \pi^+ \pi^0$  peak were 2.6%, 2.9%, and 4.2%, respectively.

Target-timing information was used to refine the delayed-coincidence requirement imposed in the trigger, providing additional rejection of in-flight decays and scattered beam pions. Further suppression of beam-pion backgrounds was achieved by rejecting events with a pion Čerenkov-counter signal in coincidence with the apparent decay pion, and by requiring the energy loss in  $B4$  to be consistent with a low-momentum  $K^+$ .

Additional rejection of photon backgrounds was obtained by summing the visible energy, excluding that of the  $\pi^+$  track, from the photon vetoes, range stack, and target, and requiring the sum to be less than 1 MeV. To minimize accidental losses, only energy in coincidence with the decay  $\pi^+$  was included in the sum. The width of the coincidence window varied with detector subsystem, but was typically 20 ns.

Muon backgrounds were suppressed by requiring that a comparison of the momentum measured in the drift chamber and the range measured in the range stack be consistent with a stopping  $\pi^+$  and by subjecting the

pulse-shape data from the stopping-counter TD's to further analysis. The pulse-shape data from both ends of the counter were fitted assuming either a single pulse, characteristic of a stopping  $\mu^+$ , or a double pulse, characteristic of a stopping  $\pi^+$  followed by  $\pi^+ \rightarrow \mu^+ \nu$  decay. Events consistent with a single pulse were rejected. Additional restrictions were placed on the fitted parameters of the double-pulse events. Specifically, we required a  $\pi \rightarrow \mu$  decay time between 9 and 120 ns, a fitted second-pulse area consistent with  $\pi^+ \rightarrow \mu^+ \nu$  decay at rest, and agreement to within  $\pm 3.5$  ns between the fitted values of the  $\pi^+ \rightarrow \mu^+ \nu$  decay times from the two ends of the counter.

Spurious signatures for  $\pi^+ \rightarrow \mu^+ \nu$  decays sometimes resulted from early  $\mu^+ \rightarrow e^+ \nu \bar{\nu}$  decays of stopped muons. Unlike the 4.1-MeV muons from pion decay at rest, electrons from muon decay usually deposited energy in several range-stack counters. We thus eliminated events with energy depositions in the vicinity of the stopping counter occurring at the same time as the apparent  $\pi \rightarrow \mu$  transition. Additional suppression came by requiring an energy deposition consistent with  $\mu^+ \rightarrow e^+ \nu \bar{\nu}$  decay in the vicinity of the stopping pion between 150 and 5000 ns after the kaon decay time.

Figure 2 shows the range-versus-kinetic-energy spectrum for charged tracks in the final sample. Only events with a measured charged-track momentum in the range  $205 < P_\pi < 243$  MeV/c are plotted. The rectangular box defines the acceptance in energy and range, and encloses the region where events from the upper portion of the  $K^+ \rightarrow \pi^+ \nu \bar{\nu}$  spectrum would fall. There are no events in the signal region. The events clustered at  $T_\pi = 108$  MeV and  $R_\pi = 30$  cm are consistent with  $K^+ \rightarrow \pi^+ \pi^0$  decays

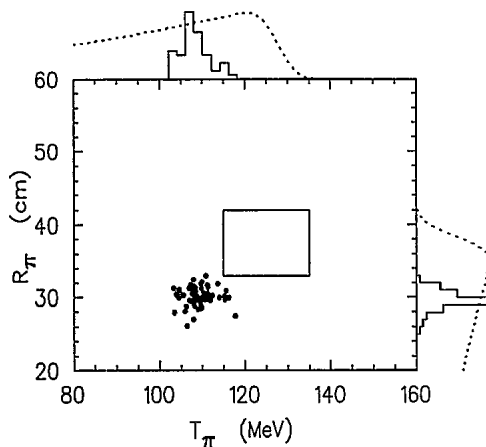


FIG. 2. Range vs kinetic energy for events satisfying the selection criteria (see text) and having measured momentum  $205 < P_\pi < 243$  MeV/c. The rectangular box indicates the search region for  $K^+ \rightarrow \pi^+ \nu \bar{\nu}$  and  $K^+ \rightarrow \pi^+ X^0$  ( $M_{X^0} = 0$ ). The dotted curves on the projection axes shows the shape of the SM spectrum for  $K^+ \rightarrow \pi^+ \nu \bar{\nu}$ , folded with the experimental resolution.

TABLE I. Acceptance factors for  $K^+ \rightarrow \pi^+ \nu \bar{\nu}$  and  $K^+ \rightarrow \pi^+ X^0$  ( $M_{X^0} = 0$ ). Each table entry represents the acceptance from a number of related cuts.

Category	$\pi^+ \nu \bar{\nu}$	$\pi^+ X^0$
Solid angle	0.47	0.47
$\pi^+$ spectrum	0.17	0.95
$\pi^+$ nuclear absorption	0.55	0.53
$\pi^+$ decay in flight	0.92	0.92
$K^+ \rightarrow \pi^+$ delayed coincidence	0.79	0.79
$\pi^+ \rightarrow \mu^+$ TD tagging	0.52	0.52
$\mu^+ \rightarrow e^+$ TD tagging	0.79	0.79
Accidental vetoes	0.70	0.69
Trigger inefficiency	0.81	0.81
Off-line reconstruction	0.74	0.73
Net acceptance	0.0055	0.029

where both photons from the  $\pi^0$  escaped detection. The 55 events correspond to a  $\pi^0$  detection inefficiency of  $1.5 \times 10^{-6}$ , consistent with Monte Carlo (MC) estimates.<sup>13</sup>

We have studied the acceptance in detail using MC simulations and calibration data sets acquired during the run. Table I summarizes the acceptance factors for  $K^+ \rightarrow \pi^+ \nu \bar{\nu}$  and for  $K^+ \rightarrow \pi^+ X^0$  when  $M_{X^0} = 0$ . The  $\pi^+$  spectrum for  $K^+ \rightarrow \pi^+ \nu \bar{\nu}$  was calculated using a SM matrix element and assuming massless neutrinos. We estimate the overall uncertainty in the acceptance to be  $\pm 10\%$ . We have checked our methods for calculating the acceptance by measuring the branching ratios for  $K^+ \rightarrow \mu^+ \nu$  and  $K^+ \rightarrow \pi^+ \pi^0$ , for which we obtained  $0.638 \pm 0.023$  and  $0.208 \pm 0.012$  (the errors are statisti-

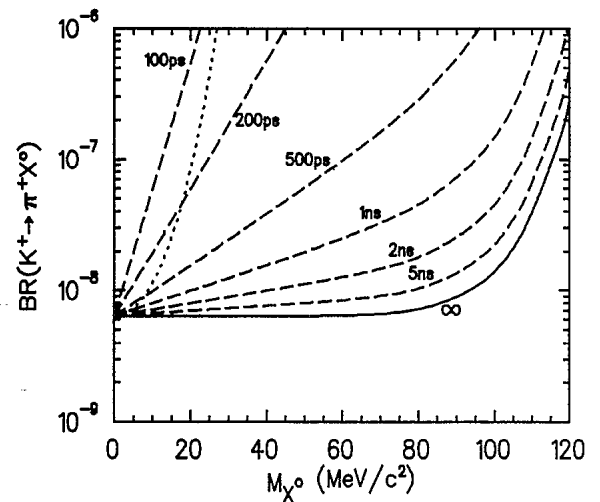


FIG. 3. The solid curve gives the 90%-C.L. upper limit on the branching ratio for  $K^+ \rightarrow \pi^+ X^0$  as a function of  $M_{X^0}$ , the mass of the recoiling system. The dashed curves give 90%-C.L. upper limits for cases where  $X^0$  has a finite lifetime. The dotted curve shows the 90%-C.L. upper limit on  $B(K^+ \rightarrow \pi^+ H^0)$  (see text).

cal), respectively, consistent with established values.<sup>14</sup>

A total of  $1.24 \times 10^{10}$  stopped kaons was acquired during a two-week period. Since no events were observed in the signal region (Fig. 2), we obtain 90%-C.L. upper limits of  $B(K^+ \rightarrow \pi^+ \nu \bar{\nu}) < 3.4 \times 10^{-8}$  and  $B(K^+ \rightarrow \pi^+ X^0) < 6.4 \times 10^{-9}$  ( $M_{X^0} = 0$ ).

Limits for  $M_{X^0} > 0$  are shown in Fig. 3. The increase of the upper limit for  $M_{X^0} > 70$  MeV/ $c^2$  reflects the falloff in acceptance for decreasing  $\pi^+$  momentum. In cases where  $X^0$  decays to detectable daughters in a finite lifetime, the limits on  $B(K^+ \rightarrow \pi^+ X^0)$  must be increased, since  $X^0$  decays in the detector volume would be vetoed. Limits for various  $X^0$  lifetimes are given by the dashed curves in Fig. 3. These curves were derived from the solid curve using two-body kinematics and the 1.5-m effective thickness of the active part of the detector. Limits can also be extracted in more complicated cases, such as a light Higgs boson in the minimal SM, which decays via  $H^0 \rightarrow e^+ e^-$  or  $H^0 \rightarrow \gamma \gamma$  and has a lifetime that depends on its mass.<sup>15</sup> The dotted curve in Fig. 3 shows the branching-ratio upper limit implied by our data in such a scenario.

Our upper limit on the branching ratio for  $K^+ \rightarrow \pi^+ \nu \bar{\nu}$  represents an approximately fourfold improvement over the previous search for this decay,<sup>5</sup> but is still well above the SM prediction. The limit on  $K^+ \rightarrow \pi^+ X^0$ , however, places constraints on various hypothetical particles and complements limits obtained from in-flight studies of the reactions  $K^+ \rightarrow \pi^+ e^+ e^-$  (Ref. 16) and  $K_L \rightarrow \pi^0 e^+ e^-$  (Ref. 17), which are most sensitive for short  $X^0$  lifetimes. In the case of the familion,<sup>8</sup> our limit suggests that the mass scale for such symmetry breaking must be of order  $7 \times 10^{10}$  GeV/ $c^2$  or higher.

We gratefully acknowledge the dedicated efforts of the technical staffs supporting this experiment and of the Brookhaven Accelerator Department. This research was supported in part by the U.S. Department of Energy under Contracts No. DE-AC02-76CH00016, No. W-7405-ENG-36, and No. DE-AC02-76ER03072, and by the Natural Sciences and Engineering Research Council

and the National Research Council of Canada.

<sup>1</sup>S. L. Glashow, J. Iliopoulos, and L. Maiani, Phys. Rev. D **2**, 1285 (1970).

<sup>2</sup>T. Inami and C. S. Lim, Prog. Theor. Phys. **65**, 297 (1981).

<sup>3</sup>J. Ellis, J. S. Hagelin, and S. Rudaz, Phys. Lett. B **192**, 201 (1987); J. Ellis, J. S. Hagelin, S. Rudaz, and D.-D. Wu, Nucl. Phys. **B304**, 205 (1988); C. O. Dib, I. Duneitz, F. J. Gilman, SLAC Report No. SLAC-PUB-4840, 1989 (to be published).

<sup>4</sup>M. Kobayashi and T. Maskawa, Prog. Theor. Phys. **49**, 652 (1973).

<sup>5</sup>Y. Asano *et al.*, Phys. Lett. **107B**, 159 (1981).

<sup>6</sup>J. Ellis and J. S. Hagelin, Nucl. Phys. **B217**, 189 (1983); M. K. Gaillard, Y. C. Kao, I.-H. Lee, and M. Suzuki, Phys. Lett. **123B**, 241 (1983); S. Bertolini and A. Masiero, Phys. Lett. **174B**, 343 (1986).

<sup>7</sup>G. B. Gelmini and M. Roncadelli, Phys. Lett. **99B**, 411 (1981). S. Bertolini and A. Santamaria, Nucl. Phys. **B315**, 558 (1989).

<sup>8</sup>F. Wilczek, Phys. Rev. Lett. **49**, 1549 (1982).

<sup>9</sup>The apparatus has been described in M. A. Selen, Ph.D. dissertation, Princeton University, 1988 (unpublished); M. Atiya *et al.*, in Proceedings of the Second International Symposium on the Fourth Family of Quarks and Leptons, Santa Monica, CA, 1989 (New York Academy of Sciences, to be published).

<sup>10</sup>J. S. Frank and R. C. Strand, in *Proceedings of the Workshop on Scintillating Fiber Detector Development for the SSC* (Fermi National Accelerator Laboratory, Batavia, IL, 1988).

<sup>11</sup>J. V. Cresswell *et al.*, IEEE Trans. Nucl. Sci. **35**, 460 (1988).

<sup>12</sup>M. Atiya *et al.*, Nucl. Instrum. Methods Phys. Res., Sect. A **279**, 180 (1989).

<sup>13</sup>This result can be used to extract limits on  $B(\pi^0 \rightarrow \nu \bar{\nu})$ . A publication on this topic is currently in preparation.

<sup>14</sup>Particle Data Group, G. P. Yost *et al.*, Phys. Lett. B **204**, 1 (1988).

<sup>15</sup>J. Ellis, M. K. Gaillard, and D. V. Nanopoulos, Nucl. Phys. **B106**, 292 (1976); L. Resnick, M. K. Sundaresan, and P. J. S. Watson, Phys. Rev. D **8**, 172 (1973).

<sup>16</sup>N. J. Baker *et al.*, Phys. Rev. Lett. **59**, 2832 (1987).

<sup>17</sup>L. K. Gibbons *et al.*, Phys. Rev. Lett. **61**, 2661 (1988).